Induced charge effects on electrokinetic entry flow

Rama Aravind Prabhakaran, Yilong Zhou, Cunlu Zhao, Guoqing Hu, Yongxin Song, Junsheng Wang, Chun Yang, and Xiangchun Xuan

---

Induced charge effects on electrokinetic entry flow

Rama Aravind Prabhakaran,[1] Yilong Zhou,[1] Cunlu Zhao,[2] Guoqing Hu,[3,4] Yongxin Song,[5] Junsheng Wang,[6] Chun Yang,[7] and Xiangchun Xuan[1,a)]

[1]*Department of Mechanical Engineering, Clemson University, Clemson, South Carolina 29634-0921, USA*
[2]*Key Laboratory of Thermo-Fluid Science and Engineering of MOE, Xi'an Jiaotong University, Xi'an 710049, China*
[3]*LNM, Institute of Mechanics, Chinese Academy of Sciences, Beijing 100190, China*
[4]*School of Engineering Science, University of Chinese Academy of Sciences, Beijing 100049, China*
[5]*College of Marine Engineering, Dalian Maritime University, Dalian 116026, China*
[6]*College of Information Science and Technology, Dalian Maritime University, Dalian 116026, China*
[7]*School of Mechanical and Aerospace Engineering, Nanyang Technological University, Singapore 639798*

Electrokinetic flow, due to a nearly plug-like velocity profile, is the preferred mode for transport of fluids (by electroosmosis) and species (by electrophoresis if charged) in microfluidic devices. Thus far there have been numerous studies on electrokinetic flow within a variety of microchannel structures. However, the fluid and species behaviors at the interface of the inlet reservoir (i.e., the well that supplies the fluid and species) and microchannel are still largely unexplored. This work presents a fundamental investigation of the induced charge effects on electrokinetic entry flow due to the polarization of dielectric corners at the inlet reservoir-microchannel junction. We use small tracing particles suspended in a low ionic concentration fluid to visualize the electrokinetic flow pattern in the absence of Joule heating effects. Particles are found to get trapped and concentrated inside a pair of counter-rotating fluid circulations near the corners of the channel entrance. We also develop a depth-averaged numerical model to understand the induced charge on the corner surfaces and simulate the resultant induced charge electroosmosis (ICEO) in the horizontal plane of the microchannel. The particle streaklines predicted from this model are compared with the experimental images of tracing particles, which shows a significantly better agreement than those from a regular two-dimensional model. This study indicates the strong influences of the top/bottom walls on ICEO in shallow microchannels, which have been neglected in previous two-dimensional models. *Published by AIP Publishing.* [http://dx.doi.org/10.1063/1.4984741]

I. INTRODUCTION

Electrokinetic flow is typically referred to as the transport of liquids by electroosmosis (EO) and the transport of (charged) species by electrophoresis (EP).[1,2] Both motions result from the action of electric field on the free charge density inside a spontaneously formed electric double layer (EDL) at the liquid-solid interface.[3,4] Electrokinetic flow is the transport method of choice in microfluidic devices because it has a much lower flow resistance and yields a much smaller hydrodynamic dispersion than the traditional pressure-driven flow.[5,6] This is attributed to its nearly plug-like velocity profile as compared to the parabolic profile of pressure-driven flow.[7] There have been numerous studies on electrokinetic flow as well as electrokinetic manipulation (e.g., mixing, focusing, pre-concentrating, and sorting) of diverse species (e.g., ions, molecules, particles, viruses, and cells) inside a variety of microchannel structures.[8–10] However, very little attention has been paid to electrokinetic entry flow from the reservoir to microchannel, which is the origin of all fluid and species motions within a microfluidic chip.

It has been reported that a continuous supply of fluid via EO induces a pressure-driven backflow inside a microchannel due to the fluid depletion and buildup in the finite-sized inlet and outlet reservoirs, respectively.[11] This phenomenon, however, becomes negligible when large reservoirs and/or long slim microchannels are used.[12] Recently our group has developed a new dielectrophoretic technique, which we termed reservoir-based dielectrophoresis (DEP)[13] for particle focusing, trapping, concentration, and separation inside the inlet reservoir in a continuous electrokinetic flow.[14,15] This technique stems from the intrinsic electric field gradients at the reservoir-microchannel junction, which is a result of the significant size mismatch between the reservoir (typically a few millimeters in diameter and depth) and microchannel (typically tens of micrometers in width and depth).[16] Its effectiveness is, however, subjected to the influence of Joule heating that may lead to a significant temperature rise in the fluid and in turn the whole microfluidic chip due to thermal diffusion.[17,18] Even worse are the resultant fluid temperature gradients at the reservoir-microchannel junction, which has been demonstrated to cause fluid circulations and hence reduce the dielectrophoretic focusing and trapping of particles.[19,20] This so-called electrothermal flow arises from the action of electric field on the inhomogeneous temperature-dependent fluid properties.[21,22] More recently, our group has reported an

---

a)Author to whom correspondence should be addressed: xcxuan@clemson.edu. Tel.: 864-656-5630. Fax: 864-656-7299.

electrokinetic in-reservoir pre-concentration of particles and bacterial cells,[23] where Joule heating effects can be safely neglected due to the use of a low ionic concentration fluid.[24,25] We have attributed this phenomenon to the recirculating flow of induced charge electroosmosis (ICEO) at the channel entrance.

Induced charge is the diffuse charge produced on a polarizable (either conducting or dielectric) surface due to the application of an electric field.[26] This charge (or, equivalently, the induced zeta potential) is different from the fixed constant charge (or, equivalently, the equilibrium zeta potential) that is acquired spontaneously on a surface in the absence of an external electric field.[27] It forms an "induced" EDL in the fluid, within which the ionic charge responds to the applied electric field yielding a fluid motion termed ICEO.[28] This flow has a nonlinear quadratic dependence on electric field and often consists of counter-rotating rolls.[29–31] It has been extensively studied around conducting surfaces of, for instance, metal electrodes and particles, which can be either electrically activated[32–34] or left floating[35–45] as reviewed by Bazant and Squires.[46] ICEO also takes place around an inert but polarizable object where the surface charge is induced by the electric field leaked into the object.[47,48] Such induced charge effects on classical EO have been studied inside microchannels with either sharp tips[49–51] or T-junctions between a wide and a narrow section.[50,52–55]

There have been a number of theoretical and numerical studies on ICEO[46,50–55] in the literature. However, the predictions from these two-dimensional (2D) models often significantly deviate from the experimental data,[50,54] sometimes even by more than one order of magnitude.[55] As the fluid and solid domains must be considered simultaneously for electric field, the three-dimensional (3D) modeling of ICEO, though expected to provide an accurate simulation, will be apparently expensive and has yet to be reported. We develop in this work for the first time a depth-averaged numerical model to predict and understand the induced charge effects on electrokinetic entry flow in microfluidic devices. This full-scale 2D simulation accounts for the influences of the top/bottom microchannel walls on charge and fluid transfer in shallow microchannels via the depth-averaging of standard transport equations. Its predictions are compared with those of a regular 2D model that assumes an infinite channel depth. We also perform a set of experiments on electrokinetic entry flow with small tracing particles in an on-chip straight rectangular microchannel. The observations are compared with the predicted particle streaklines of the depth-averaged numerical model. Moreover, a numerical parametric study is carried out on the induced charge effects in electrokinetic entry flow. The developed depth-averaged model is anticipated to serve as an efficient and accurate tool for the optimal design and control of a wide class of electrokinetic microdevices with shallow-channel geometries in a variety of applications such as sample mixing,[51] cell enrichment, and separation[14–16].

II. EXPERIMENT

A. Preparations of microfluidic chip and particle solution

Figure 1(a) shows a picture of the microfluidic chip that was fabricated with polydimethylsiloxane (PDMS) using the standard soft lithography technique. The detailed procedure can be found in our previous paper.[56] The microchip has a 2 mm-thick PDMS slab on top of a 1 mm-thick glass slide. The bottom side of the PDMS slab is a rectangular microchannel of 25 μm deep between two reservoirs. The main-body of the channel is a 500 μm-wide straight section of 3.3 cm long. Near the inlet reservoir, there is a 180 μm-long constriction with a width of 35 μm [see the inset of Fig. 1(a)], which was designed for the purpose of amplifying the local electric field. The corner radius at the junction of the reservoir and constriction was measured to be 20 μm. The two reservoirs were both made large to minimize the pressure-driven backflow. To visualize the flow pattern, 1 μm polystyrene microspheres (Polysciences, Inc.) were re-suspended in 0.01 mM phosphate buffer solution. The electric conductivity of the particle suspension was measured to be 6 μS/cm (Accumet AP85, Fisher Scientific), which is very low and ensures negligible Joule heating effects in our experiments.[24,25,56] Hence, all fluid and wall properties can be safely assumed constant and uniform in the simulation.

B. Experimental method

DC-biased AC voltages were supplied using a function generator (33220A, Agilent Technologies, Santa Clara, CA) in conjunction with a high-voltage amplifier (609 × 10^{-6}, Trek, Medina, NY). They were applied through platinum electrodes (0.5 mm diameter, Fisher) that were placed in good contact with the liquid at the inlet and outlet reservoirs. The frequency of AC voltages was fixed at 1 kHz. To avoid any pressure-driven flow, the liquid levels in the two reservoirs were
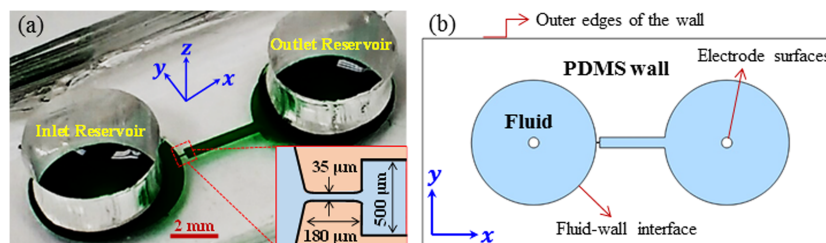
FIG. 1.   (a) Picture of the microfluidic chip (the channel and reservoirs are filled with green food dye for clarity) used in experiments. The inset is a zoom-in-view of the constriction region (not to scale) with dimensions being labeled. The (x, y) coordinates indicate the horizontal plane of the microchannel, upon which the depth-averaged analysis (i.e., along the z direction) was performed. (b) Computational domain for the depth-averaged numerical model with highlighted boundaries upon which boundary conditions are imposed for the governing equations.

carefully balanced before the start of each test. Also, all tests were run for no more than 1 min to minimize any backflow. The particle behavior at the inlet reservoir-microchannel junction was monitored using an inverted microscope imaging system (Nikon Eclipse TE2000U, Nikon Instruments) and recorded with a CCD camera (Nikon DS-Qi1Mc) at a rate of about 15 frames per second. The captured digital images were processed using the Nikon imaging software (NIS-Elements AR 2.30, Nikon Instruments, Lewisville, TX).

III. THEORY

A. Governing equations

1. Electric field

As PDMS is weakly polarizable, the electric potentials in the fluid, ϕ_f, and in the wall, ϕ_w, are solved simultaneously using the following quasi-electrostatic equations:[57]

$$\nabla \cdot \left(\sigma_f + j\omega\varepsilon_0\varepsilon_f \right) \nabla\phi_f = 0, \tag{1a}$$

$$\nabla \cdot \left(\sigma_w + j\omega\varepsilon_0\varepsilon_w \right) \nabla\phi_w = 0, \tag{1b}$$

where the two terms in each divergence represent the conduction current and displacement current, respectively. Note the convection current disappears in the fluid due to electroneutrality under the condition of a thin EDL[57] that is fulfilled in our experiments. In the above, σ is the electric conductivity of the fluid (with the subscript, f) or the wall (with the subscript, w), j is the imaginary unit, $\omega = 2\pi f$ is the angular frequency of the applied electric voltage with f being the normal frequency (fixed at 1 kHz for AC voltages in this work), ε_0 is the vacuum permittivity, and ε_f and ε_w are the relative permittivity (or dielectric constant) of the fluid and wall, respectively. Within the fluid, the displacement current is very small as compared to the conduction current because the frequency of the AC voltage used in our experiment (f = 1 kHz) is much less than the charge relaxation frequency, $\sigma_f/2\pi\varepsilon_0\varepsilon_f$ (=135 kHz).[57] Within the wall, the conduction current disappears due to the negligible electric conductivity of PDMS. Therefore, under the condition of uniform fluid and wall properties, the governing equations for electric potentials in the fluid and wall are both reduced to Laplace's equation.[57] We used the asymptotic method described in Lin *et al.*[58] to perform a depth-averaged analysis for Laplace's equation (see the supplementary material for the detailed derivation), which yields

$$\nabla_H^2 \bar{\phi}_f = 0, \tag{2a}$$

$$\nabla_H^2 \bar{\phi}_w = 0, \tag{2b}$$

where ∇_H denotes the gradient along the x and y directions in the horizontal plain of the microchannel (see Fig. 1) and $\bar{\phi}_f$ and $\bar{\phi}_w$ represent the depth-averaged electric potentials in the fluid and the PDMS wall, respectively. We use hereafter the overbar to denote a depth-averaged quantity.

2. Flow field

By dimensional analysis, we found that the Reynolds number is much smaller than 1 in our experiments, which is also typical in electrokinetic microfluidic systems.[57] Hence, the flow field, **u**, is governed by the steady-state continuity

and Stokes equations for an incompressible fluid,[57] i.e.,

$$\nabla \cdot \mathbf{u} = 0, \tag{3a}$$

$$0 = -\nabla p + \eta\nabla^2\mathbf{u}, \tag{3b}$$

where p is the pressure and η is the dynamic viscosity of the fluid. We performed a similar asymptotic analysis to Lin *et al.*[58] and obtained the following depth-averaged equations for the flow equations (see the supplementary material for the detailed derivation):

$$\nabla_H \cdot \bar{\mathbf{u}} = 0, \tag{4a}$$

$$0 = -\nabla_H\bar{p} + \eta\nabla_H^2\bar{\mathbf{u}} - 3\eta\left(\bar{\mathbf{u}} - \bar{\mathbf{u}}_{slip}\right)/d^2, \tag{4b}$$

$$\bar{\mathbf{u}}_{slip} = \left(\varepsilon_0\varepsilon_f\zeta_w/\eta\right)\nabla_H\bar{\phi}_{f\_DC}, \tag{4c}$$

where $\bar{\mathbf{u}}_{slip}$ denotes the Smoluchowski electroosmotic slip velocity[5,6] that has been assumed equal for the top and bottom channel walls with ζ_w being their equilibrium zeta potential[27] and $\bar{\phi}_{f\_DC}$ the depth-averaged DC electric potential in the fluid. The last term on the right hand side of Eq. (4b) comes from the depth-averaging with d being the half-depth of the microchannel. It accounts for the influences of the top and bottom channel walls on ICEO, which, as demonstrated below, can be very strong. This contribution is ignored in the recent work from Zehavi *et al.*,[55] where the flow field was still solved in a regular 2D model.

3. Particle tracing

The streaklines of tracing particles are determined by their relative velocity to the stationary channel walls, $\bar{\mathbf{u}}_p$, which is the vector sum of fluid velocity, $\bar{\mathbf{u}}$, electrophoretic particle velocity, $\overline{\mathbf{U}}_{EP}$, and dielectrophoretic particle velocity, $\overline{\mathbf{U}}_{DEP}$,[59]

$$\bar{\mathbf{u}}_p = \bar{\mathbf{u}} + \overline{\mathbf{U}}_{EP} + \overline{\mathbf{U}}_{DEP}, \tag{5a}$$

$$\overline{\mathbf{U}}_{EP} = -\varepsilon_0\varepsilon_f\zeta_p\nabla_H\bar{\phi}_{f\_DC}/\eta, \tag{5b}$$

$$\overline{\mathbf{U}}_{DEP} = \varepsilon_0\varepsilon_f a^2 f_{CM}\nabla\left[\left(\nabla_H\bar{\phi}_{f\_DC}\right)^2 + \left(\nabla_H\bar{\phi}_{f\_AC}\right)^2\right]/12\eta, \tag{5c}$$

where ζ_p is the particle zeta potential, f_{CM} is the Clausius-Mossotti (CM) factor,[1] a is the particle diameter, and $\bar{\phi}_{f\_AC}$ is the depth-averaged root-mean-square (RMS) AC electric potential in the fluid. Considering the low particle concentration in our experiments, the particle-particle interactions were ignored. Other contributions to particle velocity such as Brownian, inertial, and gravitational motions were also neglected.[59]

B. Computational domain and boundary conditions

Figure 1(b) shows the computational domain for our depth-averaged numerical model, which consists of the fluid and the PDMS wall in the horizontal plane of the microfluidic chip in Fig. 1(a). The two electrodes at the center of the inlet and outlet reservoirs were assumed to remain at constant electric potentials due to the platinum's high electric conductivity and hence simply treated as holes in our model.[14–16,19,56] Boundary conditions are needed for the three boundaries highlighted in Fig. 1(b) including the fluid-wall interface, electrode surfaces, and outer edges of the wall, which are explained below. Note that a symmetry boundary condition can be used

along the centerline of the microchannel that cuts the computation domain in Fig. 1(b) into half to save computational cost.

1. Electric field

The electric potential, $\phi_f = \phi_0$, is imposed upon the inlet electrode surface, where ϕ_0 is the externally applied RMS voltage. On the other electrode surface is $\phi_f = 0$ (i.e., grounded). The outer edges of the PDMS wall are all assumed insulating, $\mathbf{n} \cdot \nabla_H \bar{\phi}_w = 0$. The electric potentials inside the fluid and wall are subjected to the following boundary conditions at the fluid-wall interface:[55]

$$\bar{\phi}_w - \bar{\phi}_f = -\frac{\lambda}{\gamma^3} \frac{\varepsilon_w}{\varepsilon_f} \nabla_H \bar{\phi}_w \cdot \mathbf{n} + \zeta_w = \zeta_i + \zeta_w = \zeta, \quad (6a)$$

$$\nabla_H \bar{\phi}_f \cdot \mathbf{n} = \frac{\varepsilon_w}{\varepsilon_f} \frac{\gamma^2 - 1}{\gamma^2} \nabla_H \bar{\phi}_w \cdot \mathbf{n}, \quad (6b)$$

where ζ is the wall's overall zeta potential that consists of the polarization-induced zeta potential,[46] ζ_i, and the equilibrium zeta potential,[27] ζ_w, λ is the Debye length determined by the ionic concentration of the fluid,[27] $\gamma^2 = 1 + j\omega\lambda^2/D$ is a dimensionless quantity with D being the diffusivity that is assumed equal for positive and negative ions in the fluid, and $\mathbf{n}$ is the unit normal vector of the wall. Equation (6a) represents the electric potential jump from the fluid to the wall given by the Robin type boundary condition, which was obtained from Ref. 55 with consideration of the equilibrium zeta potential of the channel wall. Equation (6b) represents the continuity of the displacement current in the fluid and wall.[60–62] We note that for pure DC voltages, $\gamma^2 = 1$ and hence Eq. (6b) is reduced to the traditional insulating condition for electric potential in the fluid. For the AC voltages ($f = 1$ kHz) that we used in experiments, the imaginary part of γ^2, i.e., $\omega\lambda^2/D$, was estimated to be 0.06 based on $\omega = 2\pi f = 2000\pi$ Hz, $\lambda \approx 100$ nm (for 0.01 mM concentration of monovalent ions),[5,27] and $D = 1 \times 10^{-9}$ m^2/s. Therefore, we can safely assume $\gamma^2 \approx 1$ for these AC voltages, leading to essentially identical boundary conditions to those for DC voltages. For frequency much higher than 1 kHz (say, $f = 10$ kHz), however, Eq. (6b) must be used in whole and the induced zeta potential, ζ_i, apparently becomes smaller as seen from Eq. (6a). We still used the full form of Eq. (6b) to solve for the AC electric potential in this work.

2. Flow field

A no-slip condition, $\bar{\mathbf{u}} \cdot \mathbf{t} = 0$ with $\mathbf{t}$ being the unit tangential vector, is applied on each electrode surface because of the local tangential-free electric field. Due to the absence of pressure-driven flow, an equal pressure of $\bar{p} = 0$ is applied at each far end of the channel centerline that intersects with the inlet and outlet reservoirs, respectively. As the EDL thickness is very small (about 100 nm for 0.01 mM concentration of monovalent ions)[27] compared to the dimension of the channel (the smallest is the channel depth, which is 25 μm), the Smoluchowski electroosmotic slip velocity, $\bar{\mathbf{u}} \cdot \mathbf{t} = (\varepsilon_0\varepsilon_f\zeta/\eta) \nabla_H \bar{\phi}_f \cdot \mathbf{t}$, is applied on the interface between the fluid and the PDMS wall.[5,6] Further considering the induced and equilibrium parts of the wall zeta potential in Eq. (6a), we can rewrite this slip

boundary condition as

$$\bar{\mathbf{u}} \cdot \mathbf{t} = \frac{\varepsilon_0\varepsilon_f}{\eta} \left(\zeta_{i\_DC}\nabla_H \bar{\phi}_{f\_DC} + \zeta_w\nabla_H \bar{\phi}_{f\_DC} + \zeta_{i\_AC}\nabla_H \bar{\phi}_{f\_AC} \right) \cdot \mathbf{t}, \tag{7}$$

where ζ_{i_DC} and ζ_{i_AC} denote the DC and AC electric field-induced zeta potentials, respectively, that were calculated separately in our model. Note that AC field does act on the equilibrium wall zeta potential, but generates zero net electroosmotic flow.[63] In addition, a no-penetration condition, $\bar{\mathbf{u}} \cdot \mathbf{n} = 0$, is imposed upon each of the wetted surfaces.

C. Numerical method and material properties

We used commercial finite element software package, COMSOL Multiphysics 5.1 (Burlington, MA), to carry out the numerical simulation. The 2D geometry in Fig. 1(b) was created using the "Geometry" feature. The governing equations and boundary conditions for the electric and flow fields were set up in the modules "Electrostatics" and "Laminar flow," respectively. The computational domain was meshed using free triangular elements. Seven levels of mesh refinement were performed with the total number of elements being varied from about 5 000 to 1 20 000. The grid independence of the results was achieved at about 30 000 elements, where the fluid domain in the constriction region of the channel near the inlet reservoir was extremely finely meshed with a maximum element size of 2 μm. The PDMS domain was meshed with more coarse elements than the fluid domain. The depth-averaged and regular 2D models were both solved using the default solver in COMSOL. The simulation result of our regular 2D model was benchmarked against that from Zehavi *et al.*[55] for ICEO around a sharp corner under the application of AC electric field of varying frequencies.

Due to the very low electric conductivity of the fluid, the estimated temperature rise due to Joule heating is no more than 0.5 °C at the channel constriction under the highest electric field in the experiment.[57] Therefore, Joule heating effects[56] were neglected in our model, and the fluid/wall properties were all assumed uniform and constant. The equilibrium wall zeta potential, ζ_w, was determined from the electroosmotic fluid velocity that was measured using the electric current-monitoring method.[64] The particle zeta potential, ζ_p, was calculated from the electrokinetic particle velocity that

TABLE I. Summary of parameters and material properties used in the depth-averaged numerical model.[66]

Symbol	Value	Unit	Description
ε_f	80	…	Relative permittivity of fluid (i.e., water)
ε_w	4	…	Relative permittivity of PDMS wall
d	12.5	μm	Half-depth of microchannel
ζ_w	−100	mV	Equilibrium zeta potential of PDMS wall
ζ_p	−80	mV	Zeta potential of tracing particles
a	1	μm	Diameter of tracing particles
f_{CM}	+0.65	…	Clausius-Mossotti factor
λ	100	nm	Debye length
D	1×10^{-9}	m^2/s	Diffusivity of electrolyte ions
f	1	kHz	Frequency of AC voltage

was measured via single particle tracking.[14–16] The CM factor for particle DEP in Eq. (5c) was calculated from f_{CM} = $(\sigma_p - \sigma_f)/(\sigma_p + 2\sigma_f)$ for both DC and low-frequency AC voltages,[57] where the particle's electric conductivity was estimated from $\sigma_p = 4K_s/a$ with $K_s = 1$ nS as the recommended value of surface conductance for polystyrene particles.[65] For 1 μm-diameter particles, we found $\sigma_p = 40$ μS/cm and hence $f_{CM} = +0.65$ in the fluid with $\sigma_f = 6$ μS/cm. In other words, the tracing particles experienced positive DEP in our experiments and were directed towards the high-electric-field regions. Table I provides the values of the parameters and material properties used in our model.

IV. RESULTS AND DISCUSSION

A. Comparing the depth-averaged model prediction with experiment

Figure 2(a1) shows a top-view snapshot image of 1 μm tracing particles at the inlet reservoir-microchannel junction, which was taken 15 s after a 10 V DC-biased 200 V AC voltage was applied. Two counter-rotating circulations are observed at the channel entrance with one near its each corner, which is the typical feature of ICEO.[46] They are formed due to the action of electric field onto the polarization induced charge at the fluid-wall interface, which will be explained in detail in Sec. IV B. Similar to that reported in our earlier work,[23] particles get trapped inside the circulations of ICEO and are further concentrated adjacent to the corners of the channel entrance. The latter phenomenon can be better viewed from the superimposed image in Fig. 2(a2), which is a result of the action of positive DEP on particles. Figures 2(b1) and 2(b2) show the numerically predicted particle velocity vectors/contours (b1) and streaklines (b2) from the depth-averaged model under the experimental conditions, which are qualitatively consistent with the experimental images in Figs. 2(a1) and 2(a2). We note in our experiment that the majority of the particles accumulate near the two corners with only a few circulating in the vortices due to perhaps the particle-particle interactions when the local particle concentration becomes high. In contrast, the predicted circulations from a regular 2D model in the same computational domain [Figs. 2(c1) and 2(c2)] are significantly different from the experimental observation in both size and

location. This comparison indicates the strong influences of the top and bottom walls on ICEO, which has been neglected in previous studies.[50–55]

B. Understanding ICEO with the depth-averaged model

Figure 3(a) shows the numerically predicted electric field lines inside the fluid and wall domains at the inlet reservoir-microchannel junction. All conditions are identical to those described in Fig. 2. The electric field lines that leak through the dielectric corners at the channel entrance polarize the corner surfaces, leading to accumulated negative charges on the surface facing towards the reservoir (i.e., the anode side) and simultaneously positive charges on the surface facing towards the microchannel (i.e., the cathode side). In a process similar to the classical "fixed-charge" EDL,[27] such induced charges in the solid wall form an "induced" EDL in the fluid around the corners. The free ions in the induced EDL will respond to the tangential electric field yielding the so-called ICEO.[26,28] This flow is a quadratic function of electric field and hence takes place under both DC and AC electric fields. It exhibits in the form of a pair of counter-rotating vortices in front of the microchannel constriction as schematically illustrated in Fig. 3(b), which qualitatively explains why the particles get trapped and pre-concentrated by the fluid vortices in Fig. 2.

The numerically predicted distribution of the induced zeta potential, $\zeta_i = \zeta_{i\_DC} + \zeta_{i\_AC}$, along the surface of the arc corner (i.e., the fillet) is shown in Fig. 3(c), where the inset explains how the arc length is measured. For convenience, the location at which $\zeta_i = 0$ is set as the origin of the arc length. We note this "0" point is not exactly in the middle of the arc due to the asymmetry of the structure on either side of the corner. Along the positive direction of the arc length (i.e., towards the microchannel), ζ_i first increases quickly and then slowly decreases back to zero at approximately the middle of the constriction length [see the inset of Fig. 1(a)]. Along the negative direction of the arc length (i.e., towards the reservoir), ζ_i becomes negative and reaches a maximum magnitude within a short distance. Further into the negative direction of the arc length, ζ_i increases (note the magnitude decreases) very slowly and becomes zero at the far end of the inlet reservoir.
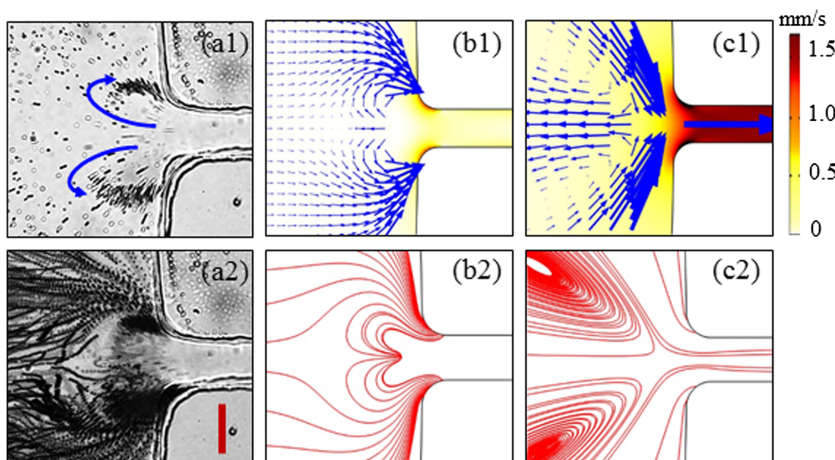

FIG. 2. Comparison of experimentally obtained images and numerically predicted trajectories of 1 μm tracing particles in electrokinetic entry flow at the inlet reservoir-microchannel junction under a 10 V DC-biased 200 V AC voltage: (a1) snapshot and (a2) superimposed images with the curved-line arrows highlighting the circulating directions of the trapped particles; (b1) predicted velocity vectors/contours and (b2) particle streaklines from the depth-averaged model; (c1) and (c2) predictions from a regular 2D model. The flow direction is from left to right in all images. The scale bar on (a2) represents 35 μm.
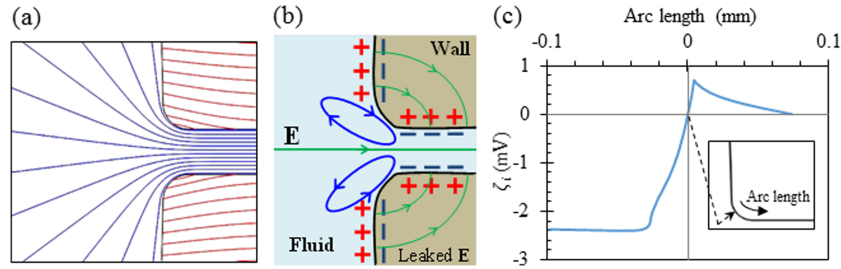
FIG. 3. Numerical understanding of the polarization-induced surface charge and the resulting ICEO at the inlet reservoir-microchannel junction in electrokinetic flow under a 10 V DC-biased 200 V AC voltage: (a) electric field lines inside the fluid (blue lines) and the PDMS wall (red line); (b) schematic diagram (not drawn to scale) showing the electric field leakage into the dielectric wall and the induced diffuse charge around the corners. The looped arrows indicate the fluid circulating directions of ICEO; (c) induced zeta potential, ζ_i, along the corner surface of the channel entrance due to the electric field leakage, where the inset shows the zoom-in-view of the arc corner on which ζ_i is plotted.

Figure 4(a) shows the predicted velocity vectors/contours (top row) and streamlines (bottom row) for the fluid EO alone at the inlet reservoir-microchannel junction in the absence of induced charge effects, i.e., the DC and AC field-induced zeta potentials, ζ_{i_DC} and ζ_{i_AC} in Eq. (7), are both set to zero. This flow is solely driven by the DC field component and follows a similar pattern to the electric field lines in the fluid in Fig. 3(a) due to the well-known similitude in pure electroosmotic flows.[67] It has a velocity of the order of 1 mm/s at near the channel entrance. The predicted velocity plots for the pure fluid ICEO, i.e., the equilibrium wall zeta potential, ζ_w, in Eq. (7) is set to zero, are displayed in Fig. 4(b). Two pairs of counter-rotating fluid circulations are observed, where the pair inside the reservoir is apparently stronger than the one inside the channel due to the larger ζ_i in the former place [see Fig. 3(c)]. This predicted pattern of ICEO is consistent with previous studies.[50–55] We note that ICEO is very weak as compared to EO and has a velocity of the order of 0.1 mm/s (the maximum magnitude is about 0.3 mm/s near the corner surfaces). Figure 4(c) shows the predicted velocity vectors/contours (top row) and streaklines (bottom row) of the tracing particles whose dielectrophoretic motion is excluded, i.e., $\overline{\mathbf{U}}_{DEP}$ in Eq. (5a) is set to zero. Particle circulations are formed only inside the reservoir and shifted towards the channel centerline, as compared to the fluid circulations of ICEO in Fig. 4(b), by DC field-driven electrokinetic flow (i.e., EO and EP). The action of positive DEP pulls the particle circulations towards the corner surfaces, as seen from Figs 2(b1) and 2(b2).

C. Examining parametric effects on induced charge in electrokinetic entry flow

1. Effect of AC voltage

Figure 5 shows the effect of AC voltage on the behavior of 1 μm tracing particles at the inlet reservoir-microchannel junction with a fixed 10 V DC bias voltage. For low values of AC voltages such as 50 V in Fig. 5(a), fluid ICEO and particle DEP are both weak. The experimentally obtained particle image (top row) agrees with the numerically predicted particle velocity vectors/contours (middle row) and streaklines (bottom row), which follow a similar pattern to the pure fluid EO in Fig. 4(a). When the AC voltage is increased to 150 V in Fig. 5(b), a small and weak vortex seems to be formed at near the front center of the channel entrance due to the increasing ICEO, which can trap part of the particles. This phenomenon is, however, not always visible unless the particle concentration gets high leading to significant particle-particle interactions. The vortex grows larger and stronger at 250 V AC in Fig. 5(c) and is split into two counter-rotating circulations that are located near the corner surfaces due to the increased influence of positive DEP. These experimental observations in Figs. 5(b) and 5(c) (top row) at increasing AC voltages are both reasonably simulated by our depth-averaged numerical model (middle and bottom rows of Fig. 5).

Figure 6 shows the numerically predicted maximum values of the induced zeta potential, ζ_i, along either corner surface
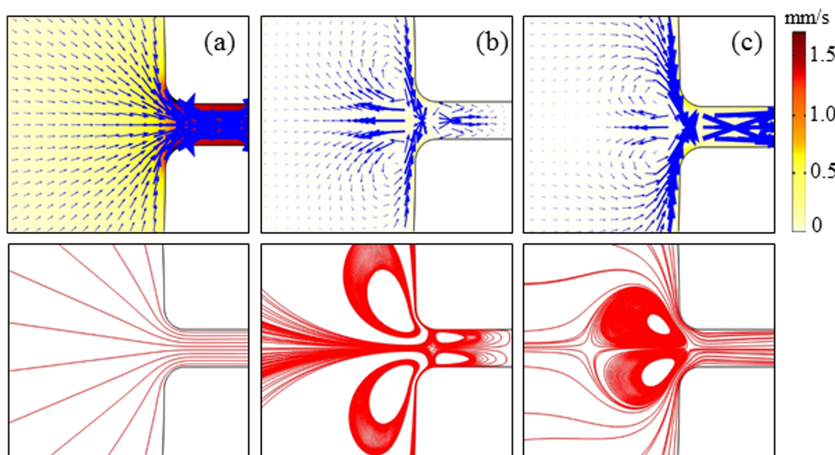

FIG. 4. Numerical understanding of induced-charge effects on electrokinetic entry flow under a 10 V DC-biased 200 V AC voltage via the predicted velocity vectors/contours (top row) and streamlines/streaklines (bottom row): (a) DC field-driven classical fluid EO alone; (b) fluid ICEO alone; (c) tracing particles without consideration of DEP.
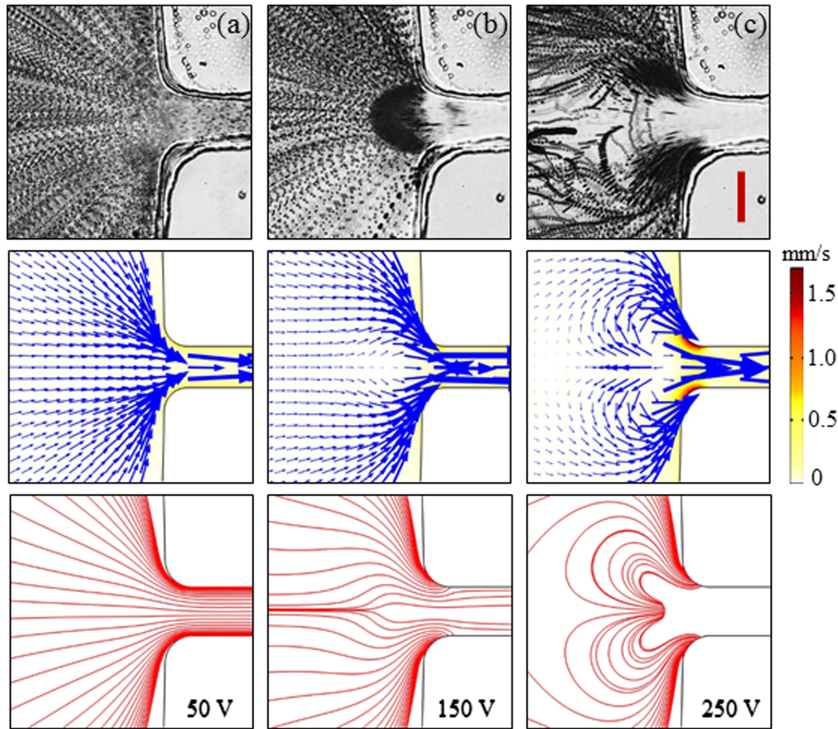
FIG. 5. Induced charge effects on electrokinetic entry flow at the inlet reservoir-microchannel junction under various 10 V DC-biased AC voltages: experimentally obtained images (top row), numerically predicted velocity vectors/contours (middle row), and streaklines (bottom row) of 1 μm tracing particles at 50 V (a), 150 V (b), and 250 V (c) AC. The flow direction is from left to right in all images. The scale bar on the image in (c) represents 35 μm.

at the channel entrance, which exhibits a nearly linear dependence on the applied AC voltage or equivalently the AC electric field. As the slip velocity at the fluid-wall interface, i.e., Eq. (7), depends linearly on the product of ζ_i and electric field, ICEO becomes a second-order function of electric field.[46] This explains why we observe stronger particle circulations with increasing AC voltage in Fig. 5. However, it should be noted that increasing DC voltage will not result in a similar effect on particle streaklines because it enhances fluid ICEO and EO simultaneously. In addition, we note that the velocity of particle DEP in Eq. (5c) is a second-order function of both electric field and particle size. Therefore, the use of smaller tracing particles can reduce the effect of particle DEP, which is expected to yield a similar behavior to those predicted particle streaklines in Fig. 4(c).
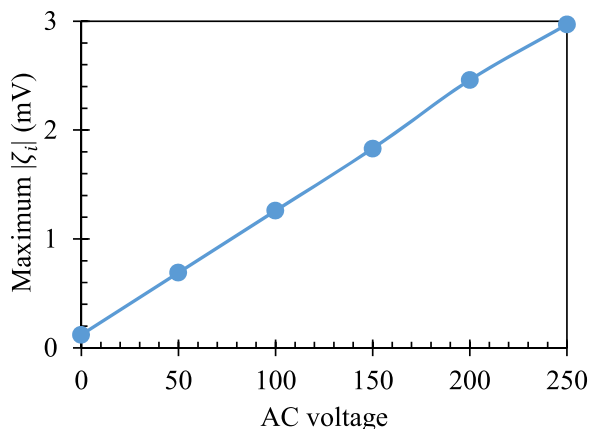

FIG. 6. AC voltage effect on the predicted maximum value of the induced zeta potential, ζ_i, along the corner surfaces at the channel entrance under a fixed 10 V DC bias voltage.

2. Effect of wall permittivity

As the induced zeta potential in Eq. (6a) has a direct dependence on the wall permittivity, ε_w, the substrate material of microfluidic chips is expected to have a strong impact on the induced charge and in turn ICEO. Figures 7(a)–7(c) show the numerically predicted streaklines of tracing particles under 10 V DC-biased 200 V AC when ε_w is varied from 2 to 4 (for PDMS in all above figures) and 6. We note these numbers are in the range of typical permittivity values for glass and other polymer based materials.[68] With a smaller value of ε_w than that for PDMS [Fig. 7(b)], the bulk of the particles experience a slight bending in their streaklines in Fig. 7(a). In contrast, with a larger value of ε_w than that for PDMS, we see in Fig. 7(c) stronger particle circulations at the channel entrance. These changes are due to the increasing magnitude of ζ_i at a higher value of ε_w as demonstrated in Fig. 7(d). The maximum value of ζ_i turns out to be a linear function of ε_w, which is consistent with its definition in Eq. (6a).

3. Effect of corner radius at the channel entrance

It has been reported that sharper dielectric corners can be more easily polarized by electric field.[49,50] This is evidenced from the exponential increase in the predicted maximum value of the induced zeta potential in Fig. 8(a) when the corner radius of the inlet reservoir-microchannel junction decreases. We note that such a trend becomes particularly steep for corner radii of less than 10 μm. Figures 8(b)–8(d) show the effect of corner radius on the predicted streaklines and velocity contours of tracing particles under a fixed voltage of 10 V DC-biased 200 V AC. The particle circulation formed near the 2 μm-radius corners is strong with a maximum vorticity of approximately 1450 s^{-1}. The latter quantity is more than one order of
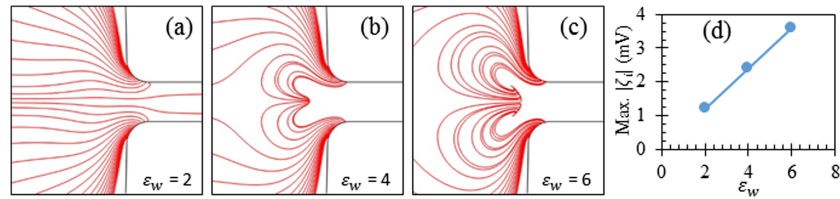
FIG. 7. Induced charge effects on electrokinetic entry flow at the inlet reservoir-microchannel junction with different values of relative permittivity for the channel wall, ε_w: ((a)–(c)) the numerically predicted streaklines of 1 μm tracing particles at $\varepsilon_w = 2$, 4, and 6, respectively; (d) the effect of ε_w on the predicted maximum value of induced zeta potential, ζ_i, along the corner surfaces at the channel entrance. The applied voltage is fixed at 10 V DC and 200 V AC. The flow direction is from left to right in all images.
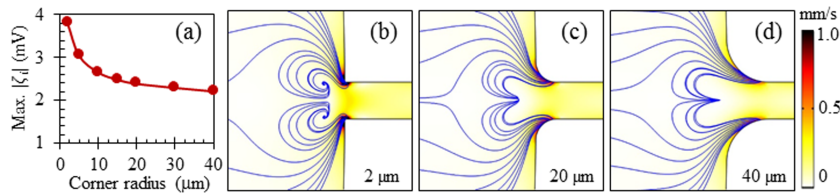

FIG. 8. Induced charge effects on electrokinetic entry flow at the inlet reservoir-microchannel junction with different corner radii: (a) the predicted maximum value of induced zeta potential, ζ_i, along the corner surfaces at the channel entrance; ((b)–(d)) the predicted streaklines and velocity contours of 1 μm tracing particles with the corner radius being 2 μm, 20 μm, and 40 μm, respectively. The applied voltage is fixed at 10 V DC and 200 V AC. The flow direction is from left to right.

magnitude higher than those for the 20 μm and 40 μm corner radii where the maximum vorticity values are only 110 s^{-1} and 60 s^{-1}, respectively. We note that particle DEP is also weakened with the increase of the corner radius due to the reduction of electric field gradients near the corner surfaces.[69,70]

V. CONCLUSIONS

We have performed a combined experimental and numerical study of induced charge effects on electrokinetic entry flow into an on-chip rectangular microchannel. It is found that the electric field leaked into the dielectric corners at the inlet reservoir-microchannel junction induces charges on the corner surfaces yielding the so-called ICEO. In conjunction with positive DEP, the recirculating flow of ICEO has been observed to trap and concentrate small tracing particles in a low ionic concentration fluid near the corners of the channel entrance. This phenomenon is reasonably captured by our depth-averaged numerical model, which uses the channel depth as a smallest parameter and takes into account the influences from the top/bottom walls of a shallow microchannel. We argue it may be the neglect of these influences that renders a regular 2D model incorrect in predicting the size, strength, and location of particle circulations. The developed depth-averaged model has also been used to study the effects of the AC voltage, wall permittivity, and corner radius on the induced charge and hence its impact on electrokinetic entry flow. The maximum value of the induced zeta potential is found to increase linearly with the AC voltage and wall permittivity while decreasing exponentially with the corner radius. For future work, we will use microparticle image velocimetry technique[71,72] to measure the fluid and (tracing) particle velocities[55] and compare them with the predictions of the depth-averaged numerical model for validation. We will also follow the analytical method developed by Yossifon and his colleagues[52,54] to conduct an asymptotic analysis of ICEO with consideration of the top and bottom wall effects.

SUPPLEMENTARY MATERIAL

See supplementary material for the depth-averaged analysis of the governing equations for electric and flow fields.

[1] H. Morgan and N. G. Green, *AC Electrokinetics: Colloids and Nanoparticles* (Research Studies Press, Philadelphia, 2002).
[2] J. H. Masliyah and S. Bhattacharjee, *Electrokinetic and Colloid Transport Phenomena* (Wiley-Interscience, 2006).
[3] R. F. Probstein, *Physicochemical Hydrodynamics*, 2nd ed. (John Willey and Sons, New York, 1994).
[4] J. Lyklemma, *Fundamentals of Interface and Colloid Science* (Academic Press, 1991).
[5] D. Li, *Electrokinetics in Microfluidics* (Elsevier Academic Press, Burlington, MA, 2004).
[6] H. C. Chang and L. Y. Yeo, *Electrokinetically Driven Microfluidics and Nanofluidics* (Cambridge University Press, New York, 2010).
[7] G. M. Whitesides and A. D. Stroock, "Flexible methods for microfluidics," Phys. Today **54**(6), 42–48 (2001).
[8] P. K. Wong, T. Wang, J. H. Deval, and C. Ho, "Electrokinetics in micro devices for biotechnology applications," IEEE/ASME Trans. Mechatron. **9**, 366–376 (2004).
[9] Y. Kang and D. Li, "Electrokinetic motion of particles and cells in microchannels," Microfluid. Nanofluid. **6**, 431–460 (2009).
[10] S. K. Srivastava, A. Gencoglu, and A. R. Minerick, "DC insulator dielectrophoretic applications in microdevice technology: A review," Anal. Bioanal. Chem. **399**, 301–321 (2010).

[11] R. J. Yang, T. I. Tseng, and C. C. Chang, "End effects on electro-osmotic flows in micro-channels," J. Micromech. Microeng. **15**, 254–262 (2005).

[12] D. Yan, C. Yang, and X. Huang, "Effect of finite reservoir size on electroosmotic flow in microchannels," Microfluid. Nanofluid. **3**, 333–340 (2007).

[13] X. Xuan, "Reservoir-based dielectrophoresis," in *Encyclopedia of Microfluidics and Nanofluidics* (Springer, 2013).

[14] S. Patel, D. Showers, P. Vedantam, T. Tzeng, S. Qian, and X. Xuan, "Microfluidic separation of live and dead yeast cells using reservoir-based dielectrophoresis," Biomicrofluidics **6**, 034102 (2012).

[15] S. Patel, S. Qian, and X. Xuan, "Reservoir-based dielectrophoresis for microfluidic particle separation by charge," Electrophoresis **34**, 961–968 (2013).

[16] J. Zhu, G. Hu, and X. Xuan, "Electrokinetic particle entry into microchannels," Electrophoresis **33**, 916–922 (2012).

[17] J. Zhu, S. Sridharan, G. Hu, and X. Xuan, "Joule heating effects on electrokinetic particle motion in insulator-based dielectrophoresis," J. Micromech. Microeng. **22**, 075011 (2012).

[18] R. Gallo-Villanueva, M. Sano, B. Lapizco-Encinas, and R. Davalos, "Joule heating effects on particle immobilization in insulator-based dielectrophoretic devices," Electrophoresis **35**, 352–361 (2014).

[19] A. Kale, S. Patel, S. Qian, G. Hu, and X. Xuan, "Joule heating effects on reservoir-based dielectrophoresis (rDEP)," Electrophoresis **35**, 721–727 (2014).

[20] A. Kale, S. Patel, G. Hu, and X. Xuan, "Numerical modeling of Joule heating effects in insulator-based dielectrophoresis microdevices," Electrophoresis **34**, 674–683 (2013).

[21] S. Sridharan, J. Zhu, G. Hu, and X. Xuan, "Joule heating effects on electroosmotic flow in insulator-based dielectrophoresis," Electrophoresis **32**, 2274–2281 (2011).

[22] B. J. Hawkins and B. J. Kirby, "Electrothermal flow effects in insulating (electrodeless) dielectrophoresis systems," Electrophoresis **31**, 3622–3633 (2010).

[23] H. Harrison, X. Lu, S. Patel, C. Thomas, A. Todd, M. Johnson, Y. Raval, T. Tzeng, Y. Song, J. Wang, D. Li, and X. Xuan, "Electrokinetic preconcentration of particles and cells in microfluidic reservoirs," Analyst **140**, 2869–2875 (2015).

[24] B. Cetin and D. Li, "Effect of Joule heating on electrokinetic transport," Electrophoresis **29**, 994–1005 (2008).

[25] X. Xuan, "Joule heating in electrokinetic flow," Electrophoresis **29**, 33–43 (2008).

[26] M. Z. Bazant and T. M. Squires, "Induced-charge electrokinetic phenomena: Theory and microfluidic applications," Phys. Rev. Lett. **92**, 066101 (2004).

[27] R. J. Hunter, *Zeta Potential in Colloid Science* (Academic Press, New York, 1981).

[28] T. M. Squires and M. Z. Bazant, "Induced-charge electro-osmosis," J. Fluid Mech. **509**, 217–252 (2004).

[29] A. Ramos, H. Morgan, N. G. Green, and A. Castellanos, "AC electric-field-induced fluid flow in microelectrodes," J. Colloid Interface Sci. **217**, 420–422 (1999).

[30] N. G. Green, A. Ramos, A. González, H. Morgan, and A. Castellanos, "Fluid flow induced by nonuniform AC electric fields in electrolytes on microelectrodes. I. Experimental measurements," Phys. Rev. E **61**, 4011 (2000).

[31] J. A. Levitan, S. Devasenathipathy, V. Studer, Y. Ben, T. Thorsen, T. M. Squires, and M. Z. Bazant, "Experimental observation of induced-charge electro-osmosis around a metal wire in a microchannel," Colloids Surf., A **267**, 122–132 (2005).

[32] A. Ajdari, "Pumping liquids using asymmetric electrode arrays," Phys. Rev. E **61**, R45–R48 (2000).

[33] P. K. Wong, C. Y. Chan, T. H. Wang, and C. M. Ho, "Electrokinetic bioprocessor for concentrating cells and molecules," Anal. Chem. **76**, 6908–6914 (2004).

[34] C. C. Huang, M. Z. Bazant, and T. Thorsen, "Ultrafast high-pressure AC electro-osmotic pumps for portable biomedical microfluidics," Lab Chip **10**, 80–85 (2010).

[35] E. Yariv, "Induced-charge electrophoresis of non-spherical particles," Phys. Fluids **17**, 051702 (2005).

[36] T. M. Squires and M. Z. Bazant, "Breaking symmetries in induced-charge electro-osmosis and electrophoresis," J. Fluid Mech. **560**, 65–101 (2006).

[37] H. Zhao and H. Bau, "Microfluidic chaotic stirrer utilizing induced-charge electro-osmosis," Phys. Rev. E **75**, 066217 (2007).

[38] H. Zhao and H. Bau, "On the effect of induced electro-osmosis on a cylindrical particle next to a surface," Langmuir **23**, 4053–4063 (2007).

[39] M. Abu Hamed and E. Yariv, "Induced-charged electrokinetic flows about polarizable nano-particles: The thick-Debye-layer limit," J. Fluid Mech. **627**, 341–360 (2009).

[40] S. E. Yalcin, A. Sharma, S. Qian, S. W. Joo, and O. Baysal, "Manipulating particles in microfluidics by floating electrodes," Electrophoresis **31**, 3711–3718 (2010).

[41] M. S. Kilic and M. Z. Bazant, "Induced-charge electrophoresis near a wall," Electrophoresis **32**, 614–628 (2011).

[42] O. Schnitzer and E. Yariv, "Induced-charge electro-osmosis beyond weak fields," Phys. Rev. E **86**, 061506 (2012).

[43] Y. Ren, W. Liu, Y. Jia, Y. Tao, J. Shao, Y. Ding, and H. Jiang, "Induced-charge electroosmotic trapping of particles," Lab Chip **15**, 2181–2191 (2015).

[44] H. Feng, T. N. Wong, and Z. Che, "Induced charge electrophoresis of a conducting cylinder in a nonconducting cylindrical pore and its micromotoring application," Phys. Rev. Fluids **1**, 044103 (2016).

[45] Y. Ren, W. Liu, J. Liu, Y. Tao, Y. Guo, and H. Jiang, "Particle rotational trapping on a floating electrode by rotating induced-charge electroosmosis," Biomicrofluidics **10**, 054103 (2016).

[46] M. Z. Bazant and T. M. Squires, "Induced-charge electrokinetic phenomena," Curr. Opin. Colloid Interface Sci. **15**, 203–213 (2010).

[47] S. K. Thamida and H. C. Chang, "Nonlinear electrokinetic ejection and entrainment due to polarization at nearly insulated wedges," Phys. Fluids **14**, 4315 (2002).

[48] F. Nadal, F. Argoul, P. Kestener, B. Pouligny, C. Ybert, and A. Ajdari, "Electrically induced flows in the vicinity of a dielectric stripe on a conducting plane," Eur. Phys. J. E: Soft Matter **9**, 387–399 (2002).

[49] J. K. Chen and R. J. Yang, "Vortex generation in electroosmotic flow passing through sharp corners," Microfluid. Nanofluid. **5**, 719–725 (2008).

[50] Y. Eckstein, G. Yossifon, A. Seifert, and T. Miloh, "Nonlinear electrokinetic phenomena around nearly insulated sharp tips in microflows," J. Colloid Interface Sci. **338**, 243–249 (2009).

[51] P. Takhistov, K. Duginova, and H.-C. Chang, "Electrokinetic mixing vortices due to electrolyte depletion at microchannel junctions," J. Colloid Interface Sci. **263**, 133–143 (2003).

[52] G. Yossifon, I. Frankel, and T. Miloh, "On electro-osmotic flows through microchannel junctions," Phys. Fluids **18**, 117108 (2006).

[53] J. D. Sherwood, M. Mao, and S. Ghosal, "Electrically generated eddies at an eightfold stagnation point within a nanopore," Phys. Fluids **26**, 112004 (2014).

[54] M. Zehavi and G. Yossifon, "Particle dynamics and rapid trapping in electro-osmotic flow around a sharp microchannel corner," Phys. Fluids **26**, 082002 (2014).

[55] M. Zehavi, A. Boymelgreen, and G. Yossifon, "Competition between induced-charge electro-osmosis and electrothermal effects at low frequencies around a weakly polarizable microchannel corner," Phys. Rev. Appl. **5**, 044013 (2016).

[56] R. A. Prabhakaran, Y. Zhou, S. Patel, A. Kale, Y. Song, G. Hu, and X. Xuan, "Joule heating effects on electroosmotic entry flow," Electrophoresis **38**, 572–579 (2017).

[57] A. Castellanos, A. Ramos, A. Gonzalez, N. G. Green, and H. Morgan, "Electrohydrodynamics and dielectrophoresis in microsystems: Scaling laws," J. Phys. D: Appl. Phys. **36**, 2584–2597 (2003).

[58] H. Lin, B. D. Storey, and J. G. Santiago, "A depth-averaged electrokinetic flow model for shallow microchannels," J. Fluid Mech. **608**, 43–70 (2008).

[59] N. G. Green, A. Ramos, and H. Morgan, "AC electrokinetics: A survey of sub-micrometre particle dynamics," J. Phys. D: Appl. Phys. **33**, 632–641 (2000).

[60] C. Zhao and C. Yang, "AC field induced-charge electroosmosis over leaky dielectric blocks embedded in a microchannel," Electrophoresis **32**, 629–637 (2011).

[61] G. Yossifon, I. Frankel, and T. Miloh, "Macro-scale description of transient electro-kinetic phenomena over polarizable dielectric solids," J. Fluid Mech. **620**, 241–262 (2009).

[62] C. Zhao and C. Yang, "Analysis of induced-charge electro-osmotic flow in a microchannel embedded with polarizable dielectric blocks," Phys. Rev. E **80**, 046312 (2009).

[63] X. Xuan and D. Li, "Electroosmotic flow in microchannels with arbitrary geometry and arbitrary distribution of wall charge," J. Colloid Interface Sci. **289**, 291–303 (2005).

[64] A. Sze, D. Erickson, L. Ren, and D. Li, "Zeta-potential measurement using the Smoluchowski equation and the slope of the current–time relationship in electroosmotic flow," J. Colloid Interface Sci. **261**, 402–410 (2003).

[65] I. Ermolina and H. Morgan, "The electrokinetic properties of latex particles: Comparison of electrophoresis and dielectrophoresis," J. Colloid Interface Sci. **285**, 419–428 (2005).

[66] D. R. Lide, *CRC Handbook of Chemistry and Physics*, 90th ed. (CRC Press, Boca Raton, FL, 2009).

[67] J. G. Santiago, "Electroosmotic flows in microchannels with finite inertial and pressure forces," Anal. Chem. **73**, 2353–2365 (2001).

[68] F. Zhang and D. Li, "Induced-charge electroosmotic flow around dielectric particles in uniform electric field," J. Colloid Interface Sci. **410**, 102–110 (2013).

[69] J. Zhu and X. Xuan, "Particle electrophoresis and dielectrophoresis in curved microchannels," J. Colloid Interface Sci. **340**, 285–290 (2009).

[70] Y. Ai, S. Park, J. Zhu, X. Xuan, A. Beskok, and S. Qian, "DC electrokinetic particle transport in an L-shaped microchannel," Langmuir **26**, 2937–2944 (2010).

[71] D. Wang, M. Sigurdson, and C. D. Meinhart, "Experimental analysis of particle and fluid motion in AC electrokinetics," Exp. Fluids **38**, 1–10 (2005).

[72] S. T. Wereley and C. D. Meinhard, "Recent advances in micro-particle image velocimetry," Annu. Rev. Fluid Mech. **42**, 557–576 (2010).